Secretagogin marks amygdaloid PKCδ interneurons and modulates NMDA receptor availability

Zsófia Hevesi[a,b,c], Dóra Zelena[d,e], Roman A. Romanov[c], János Hanics[a,b], Attila Ignácz[f], Alice Zambon[g], Daniela D. Pollak[g], Dávid Lendvai[b], Katalin Schlett[f], Miklós Palkovits[h], Tibor Harkany[c,i], Tomas G. M. Hökfelt[i,1], and Alán Alpár[a,b,1]

[a]SE-NAP Research Group of Experimental Neuroanatomy and Developmental Biology, Hungarian Academy of Sciences, H-1094 Budapest, Hungary; [b]Department of Anatomy, Semmelweis University, H-1094 Budapest, Hungary; [c]Department of Molecular Neurosciences, Center for Brain Research, Medical University of Vienna, A-1090 Vienna, Austria; [d]Behavioral Neurobiology, Institute of Experimental Medicine, Hungarian Academy of Sciences, H-1083 Budapest, Hungary; [e]Centre for Neuroscience, Szentágothai Research Centre, Institute of Physiology, Medical School, University of Pécs, H-7624 Pécs, Hungary; [f]Neuronal Cell Biology Research Group, Department of Physiology and Neurobiology, Eötvös Loránd University, H-1117 Budapest, Hungary; [g]Department of Neurophysiology and Neuropharmacology, Medical University of Vienna, A-1090 Vienna, Austria; [h]Human Brain Tissue Bank and Laboratory, Semmelweis University, H-1094 Budapest, Hungary; and [i]Department of Neuroscience, Biomedicum D0776, Karolinska Institutet, SE-17165 Solna, Sweden

Contributed by Tomas G. M. Hökfelt, December 17, 2020 (sent for review December 2, 2019; reviewed by Alon Amir, Marco Capogna, and Joseph E. LeDoux)

The perception of and response to danger is critical for an individual's survival and is encoded by subcortical neurocircuits. The amygdaloid complex is the primary neuronal site that initiates bodily reactions upon external threat with local-circuit interneurons scaling output to effector pathways. Here, we categorize central amygdala neurons that express secretagogin (Scgn), a Ca^{2+}-sensor protein, as a subset of protein kinase Cδ $(PKCδ)^{+}$ interneurons, likely "off cells." Chemogenetic inactivation of $Scgn^{+}/PKCδ^{+}$ cells augmented conditioned response to perceived danger in vivo. While Ca^{2+}-sensor proteins are typically implicated in shaping neurotransmitter release presynaptically, Scgn instead localized to postsynaptic compartments. Characterizing its role in the postsynapse, we found that Scgn regulates the cell-surface availability of NMDA receptor 2B subunits (GluN2B) with its genetic deletion leading to reduced cell membrane delivery of GluN2B, at least in vitro. Conclusively, we describe a select cell population, which gates danger avoidance behavior with secretagogin being both a selective marker and regulatory protein in their excitatory postsynaptic machinery.

associative learning | calcium-binding protein | limbic system | fear conditioning

The amygdala is a brain structure critical for the acquisition and relay of threatening stimuli to execute behavioral responses to danger (1, 2). Much of our understanding about this process is based on the concept of internuclear lateral-to-medial information flow within the amygdaloid complex, with the lateral (LA) and central (CeA) amygdaloid nuclei being the main input and output, respectively (3). During the acquisition of experience-induced danger responses, unconditioned threat and context-specific environmental cues are linked in the basolateral amygdaloid nucleus, anterior part (BLA) (4). In turn, the CeA serves as a relay and processes information via its local recurrent inhibitory circuits before feeding those toward effector structures (5–7), including the prefrontal cortex (8). Instead of being a passive relay station, the CeA is likely to participate in the learning of danger responses (9–13): Anatomical and physiological evidence converge to indicate that output neurons in the medial part of the CeA (CeM) are under inhibitory control, which originates in its lateral subregion (CeL) (5, 12, 14, 15). In accord with this principle, neuronal subsets specific for the different CeA subnuclei were identified and causally related to the regulation of danger avoidance behavior (10). In the CeL, PKCδ-positive$^{(+)}$ ("fear-off") neurons project onto and inhibit CeM output neurons that trigger danger-induced behavior, such as freezing (10). In turn, "fear-on" CeL neurons marked by the expression of the neuropeptide somatostatin (SOM^{+}) modulate afferent and efferent signals locally within the CeL or via inhibitory connections between CeL and CeM, probably involving neuropeptide-Y Y2 receptors (16). Additionally, these CeL neurons form mutual inhibitory connections with corticotropin releasing hormone $(CRH)^{+}$ neurons, which determine the balance between conditioned flight and fright (freezing) behaviors (17). While fear-on neurons suppress fear-off neurons, both cell types receive direct excitatory input from the LA (18). Based on these wiring principles, a series of studies have charted the cellular constituents of threat-responsive CeA circuits, with cell type-specific genetic manipulations allowing for inferences to be made toward fear-related disorders (9). Nevertheless, molecular mechanisms specific to distinct interneuron subclasses amenable to gating behavioral responses remain less well explored.

Ca^{2+} plays critical roles in determining the physiology of synaptic neurotransmission. Upon synaptic activity, Ca^{2+} entry activates Ca^{2+}-sensor proteins to trigger cell state- and context-specific intracellular signaling events by recruiting partner proteins in signalosome complexes (19). Secretagogin (Scgn) is one such Ca^{2+}-sensor protein whose expression is activity dependent (20) and specific to a hitherto undefined GABA interneuron

Significance

Unconscious reactions to threat orchestrated by subcortical brain structures are critical to save the individual at peril. The innate behavioral responses can be modulated by associative learning processes in which the amygdaloid complex gates active motor commands to avoid danger. At the cellular level, glutamatergic neurotransmission through postsynaptic NMDA receptors drives threat-induced changes in synaptic function. Here, we show that the availability of NMDA receptors in the postsynapse is modulated by secretagogin, a Ca^{2+} sensor protein. Chemogenetic inactivation of secretagogin-expressing neurons, or ablation of secretagogin itself, provides causality for the role of Ca^{2+}-dependent feedback regulation at the cellular level.

Author contributions: D.Z., D.D.P., K.S., M.P., T.H., T.G.M.H., and A.A. designed research; Z.H., D.Z., R.A.R., J.H., A.I., A.Z., D.D.P., D.L., and A.A. performed research; M.P. and T.H. contributed new reagents/analytic tools; Z.H., R.A.R., J.H., A.I., A.Z., D.D.P., D.L., K.S., T.G.M.H., and A.A. analyzed data; and Z.H., T.H., T.G.M.H., and A.A. wrote the paper.

Reviewers: A.A., Rutgers University; M.C., University of Aarhus; and J.E.L., New York University.

The authors declare no competing interest.

[1]To whom correspondence may be addressed. Email: Tomas.Hokfelt@ki.se or alpar.alan@med.semmelweis-univ.hu.

This article contains supporting information online at https://www.pnas.org/lookup/suppl/doi:10.1073/pnas.1921123118/-/DCSupplemental.

Published February 8, 2021.

subclass in the CeL (21). However, the role of Scgn in the amygdala remains unknown.

Here, we hypothesized that Scgn could modulate excitatory neurotransmission locally to scale behavioral responses in danger. By combining classical neuroanatomy, neurochemistry, electrophysiology, and behavioral genetics, we found that Scgn marks a subpopulation of PKCδ$^+$ CeL interneurons whose inhibition triggers freezing in a typical behavioral paradigm for the assessment of danger responses in rodents, termed "fear conditioning" (15, 22). Ultrastructural analysis showed Scgn enrichment in the subsynaptic region of dendrites apposing excitatory afferents, which was biochemically confirmed by synaptic fractionation and Western blotting. Postsynaptic localization is unexpected because the bulk of studies on Scgn implicates this Ca^{2+}-sensor protein in presynaptic neurotransmitter release. By reanalyzing our open-source proteomics data, we identified the 2B subunit of the NMDA receptor (GluN2B) as a stable member of the Scgn signalosome, confirmed a putative protein–protein interaction by immunoprecipitation, and thus suggest a role for Scgn in shaping GluN2B surface availability by using fluorescence recovery after photobleaching (FRAP) combined with gene silencing in vitro. These data suggest that Scgn$^+$ CeL neurons are central to gate danger responses with Scgn contributing to the assembly of the excitatory postsynaptic machinery at the cell membrane.

Results

Secretagogin Labels Interneurons in CeL. Scgn$^+$ neurons exist in several divisions of the rat amygdala (*SI Appendix*, Fig. S1) with a focal accumulation in the CeL (Fig. 1*A*). Morphological, tract-tracing, and ultrastructural findings in rat suggest that Scgn$^+$ neurons are interneurons: 1) their somata are multipolar or ovoid and their dendrites smooth (*SI Appendix*, Fig. S2) or sparsely spiny (Fig. 1*B*), which are typical phenotypic attributes of interneurons in the rodent amygdala (23); 2) Scgn was found in the presynaptic compartment of symmetrical synapses at the ultrastructural level (Fig. 1*C*, taken from CeL), labeling inhibitory synapses; 3) viral tracing in *Scgn*-Cre mice with pAAV8-hSyn-DIO-mCherry particles injected into the CeL led us to visualize local axonal arbors within the CeL (Fig. 1 *D* and D_1); 4) when performing in vivo retrograde tracing by biotinylated dextran amine (BDA) from major target areas of the CeL and BLA, including the nucleus accumbens (Fig. 1 E–E_3), striatum and the bed nucleus of stria terminalis (BNST) (*SI Appendix*, Fig. S3), we identified the complementary distribution of BDA$^+$/Scgn$^-$ and BDA$^-$/Scgn$^+$ neurons within the CeL. Likewise, when mapping Scgn$^+$ neurons in both rostral and caudal parts of the human amygdala (by means of Neurolucida), we found them at highest density in the CeL division (Fig. 1 *F* and F_1 and *SI Appendix*, Fig. S4). Cumulatively, these morphological features suggest inhibitory interneuron (or local-circuit neuron) identity.

We hypothesized that Scgn is involved in danger response-related events but not in stress situations that lack a conditioning stimulus. CeL harbors CRH$^+$ neurons, which regulate responses in acute restraint stress (24) and stressor-triggered behaviors (25). We used CRH-GFP mice (n = 3) (26) to show that Scgn$^+$ neurons lacked CRH but formed a mutually exclusive population with CRH$^+$ cells (Fig. 1 *G* and G_1"), the latter being typically activated by unconditioned stress (10), excluding the possibility of an extrahypothalamic "stress-axis" cell group. Scgn$^+$ neurons did not become activated by acute pain-evoked stress: formalin injection into the paw of adult rats (n = 4) triggered the activation of stress-sensitive central amygdala neurons (27), which, however, lacked Scgn expression (20 min postinjection; Fig. 1 H–H_1"). Instead, Scgn$^+$ neurons typically coexpressed PKCδ$^+$ (Fig. 1 I–I"): while 26.64 ± 2.33% of all PKCδ$^+$ neurons coexpressed Scgn, 92.36 ± 1.51% of all Scgn$^+$ neurons were PKCδ$^+$ (n = 3 animals). Of note, inhibition/excitation of PKCδ$^+$ CeL neurons trigger behavioral responses during fear conditioning (10). We thus used current clamp recording in Scgn-GFP mice to determine some electrophysiological characteristics of Scgn$^+$ CeL neurons. Previously, PKCδ$^+$ CeL neurons were classified as late-firing cells (10). Indeed, the majority (92%, 12 out of 13 cells, from n = 3 animals) of Scgn$^+$ CeL neurons showed identical characteristics with a resting membrane potential Rm = −71.1 ± 1.23 mV, input resistance IR = 326.8 ± 45.07, and a threshold potential of 60 ± 9.95 mV (Figs. 1 *J* and *J*' and 2*E*), as measured in acute brain slices of young-adult mice.

Scgn Labels Fear-Off Neurons. We then chose a chemogenetic approach to test the function of Scgn$^+$ neurons in the CeL by injecting AAV particles carrying Cre-dependent DREADD expression systems for neuronal activation (hM3Dq, ref. 28; in n = 8 animals) or inactivation (hM4Di, ref. 29; in n = 5 animals), or for control (hSyn in n = 5 animals) into the CeL of *Scgn*-Cre mice (Fig. 2 *A*–*B*'). We used a classical Pavlovian aversive conditioning procedure, during which we paired the presentation of a tone with a foot-shock serving as conditioned and unconditioned stimuli, respectively (*SI Appendix*, Fig. S5 *A*–A_1'). Exposing CNO-pretreated animals (30 min; 1 mg/kg body weight) to contextual fear conditioning, we found that chemogenetic inhibition of Scgn$^+$ neurons increased freezing time (Fig. 2*C*; P < 0.05, Student's t test) and, coincidently, reduced the distance the animals moved in their cages after conditioning (Fig. 2*C*'; P < 0.05, Student's t test). These results support that Scgn$^+$ CeL neurons form a population of PKCδ$^+$ CeL cells, which were previously described to block fear-evoked behavior (10) (Fig. 2*D*).

In behavioral paradigms, plastic changes among CeL interneurons were attributed to SOM$^+$ cell while their downstream target PKCδ$^+$ CeL neurons are known to exert tonic inhibition on CeM neurons and convey disinhibition from CeL in danger response behavior (7). We found that lack of Scgn does not change the electrophysiological properties of Scgn$^+$/PKCδ$^+$ CeL neurons. Input resistance, threshold potential, the minimal frequency of action potentials, and neuronal resting potential did not change in *Scgn*$^{-/-}$ mice compared to wild-type (WT) control mice (Fig. 2*E*). Further, genetic ablation of Scgn did not change the proportion of functionally active NMDA receptors vs. AMPA channels (30) in late-firing neurons of the central amygdala after fear conditioning (Fig. 2 *F* and F_1); we showed this by measuring EPSC evoked by extracellular stimulation at different holding potentials (−80 and +60), where no genotype effect was identified (n = 14 cells and n = 10 cells in WT and *Scgn*$^{-/-}$ mice, respectively, Mann–Whitney rank-sum test). Animals of both genotypes were able to acquire a cued fear response as evidenced by a significantly increased percentage of time spent freezing during the presentation of the conditioned stimulus (CS), as compared to the equvivalent time period before the onset of the CS. No differences between *Scgn*$^{-/-}$ and WT controls were detected (Fig. 2*G*; n = 5 KO and n = 9 WTs, P = 0.24, ANOVA, Student's t test).

Secretagogin Is Expressed in Excitatory Postsynapses. Scgn has typically been localized to presynaptic terminals and implicated in regulating vesicular exocytosis (19, 20, 31, 32). Within the amygdala, we also find symmetrical synapses with Scgn-laden presynaptic terminals (Fig. 1*C*). Indirect evidence for a postsynaptic expression site was obtained in Western blotting experiments, where Scgn was detected in in total and postsynaptic fractions after differential centrifugation of amygdala micropunches (Fig. 3*A*). Scgn's presence in the postsynaptic compartment prompted us to interrogate its potential function associated with the postsynaptic signal transduction machinery. We hypothesized that Scgn might interact with a specific ion channel. Therefore, we have reprocessed our open-source

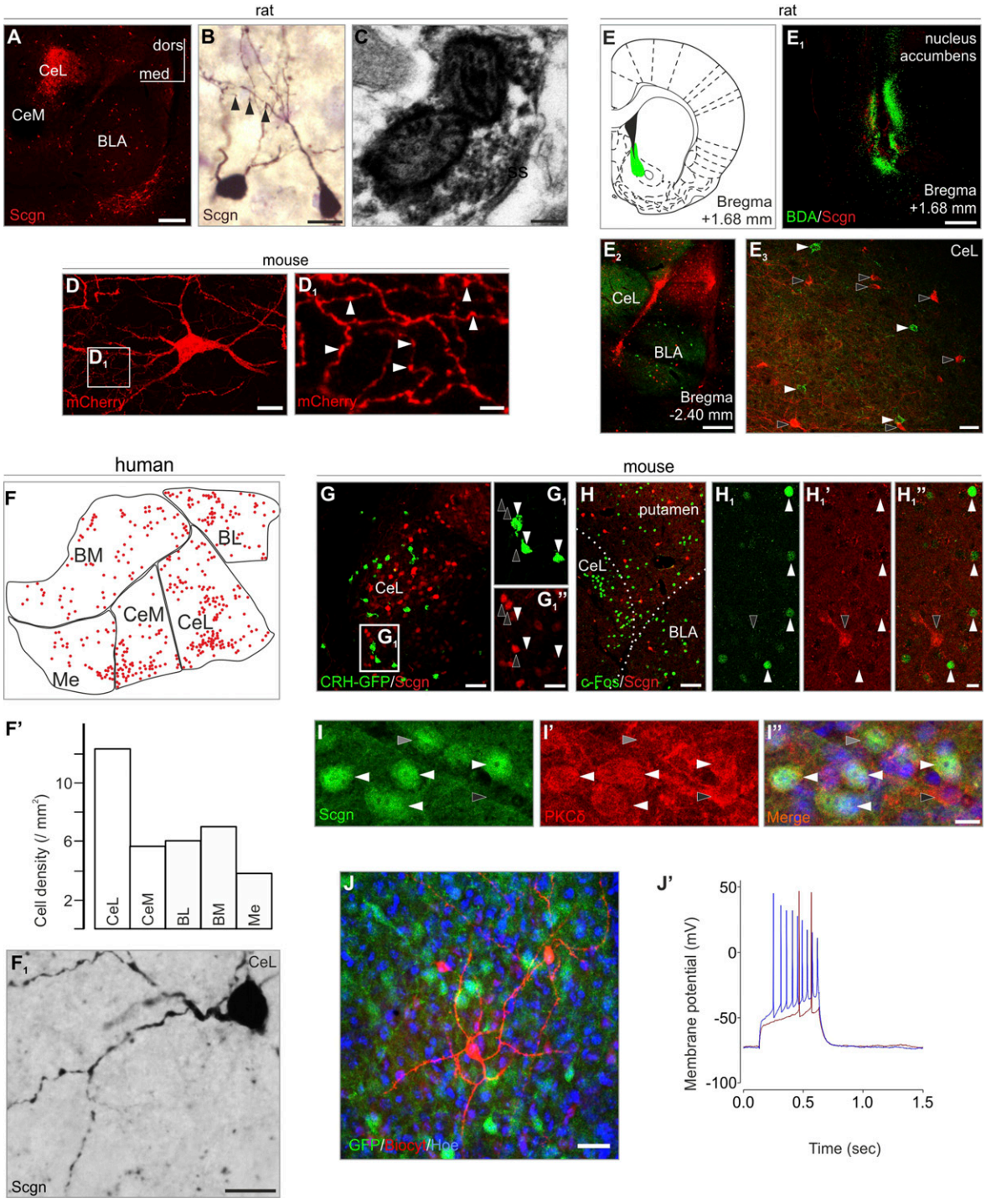

Fig. 1. Secretagogin (Scgn) labels interneurons in the amygdala. (*A*) Scgn$^+$ neurons typically populated the CeL (for schemata of representative coronal sections and complete amygdala survey see *SI Appendix*, Fig. S1). (*B*) Scgn$^+$ neurons were typically multipolar with spines occasionally observable on their dendrites (arrowheads). (*C*) Scgn in the presynaptic compartment of a symmetrical synapse. (*D* and *D_1*) mCherry-labeled interneuron in a *Scgn*-Cre mouse microinjected with pAAV8-hSyn-DIO-mCherry virus in the CeL. Arrowheads point to varicosities in the local axonal arbour. (*E*–*E_3*) BDA$^+$ retrogradely labeled neurons (tracer injection: nucleus accumbens) remained Scgn$^-$ in the CeL. (*F*–*F_1'*) In human, Scgn$^+$ neurons appeared in highest density in the CeL. (*G*–*G_1''*) Scgn$^+$ neurons (open arrowheads) and CRH-GFP$^+$ neurons (filled arrowheads) exhibited complementary distribution in the amygdala when using CRH-GFP transgenic mice. (*H*–*H_1''*) Formalin stress induced c-Fos expression in Scgn$^-$ neurons (filled arrowheads). Open arrowhead points to a Scgn$^+$ neuron. (*I*–*I''*) Scgn$^+$ neurons typically coexpress PKCδ (white arrowheads point to Scgn$^+$/PKCδ$^+$ neurons; gray and black arrowheads indicate Scgn$^+$/PKCδ$^-$ and secretagogin$^-$/PKCδ$^+$ somata, respectively. (*J* and *J'*) Whole-cell patch clamp recordings and cell reconstruction in amygdala slices of Scgn-GFP animals. Step current injections produced representative voltage changes in Scgn-GFP$^+$ cells with delayed generation of the first action potential (12 of 13 cells). *A* and *E_2* were captured by using the tile-and-stitch function of the ZEN2012 imaging toolbox (Zeiss). BL, basolateral amygdaloid nucleus (human); BM, basomedial amygdaloid nucleus (human); BLA, basolateral amygdaloid nucleus, anterior part (mouse and rat); CeM, central amygdaloid nucleus, medial division (human and rat); CeL, central amygdaloid nucleus, lateral division (human, mouse, and rat); dors, dorsal; med, medial; Me, medial amygdaloid nucleus (human); ss, symmetrical synapse. (Scale bars: *A*, *E_1*, and *E_2*, 500 μm; *C*, 200 nm; *B*, *D*, *F_1'*, *H_1''*, *I*, and *J*, 15 μm; *D_1*, 4 μm; *E_3* and *G*, 50 μm; *G_1''*, 20 μm; *H*, 80 μm.)

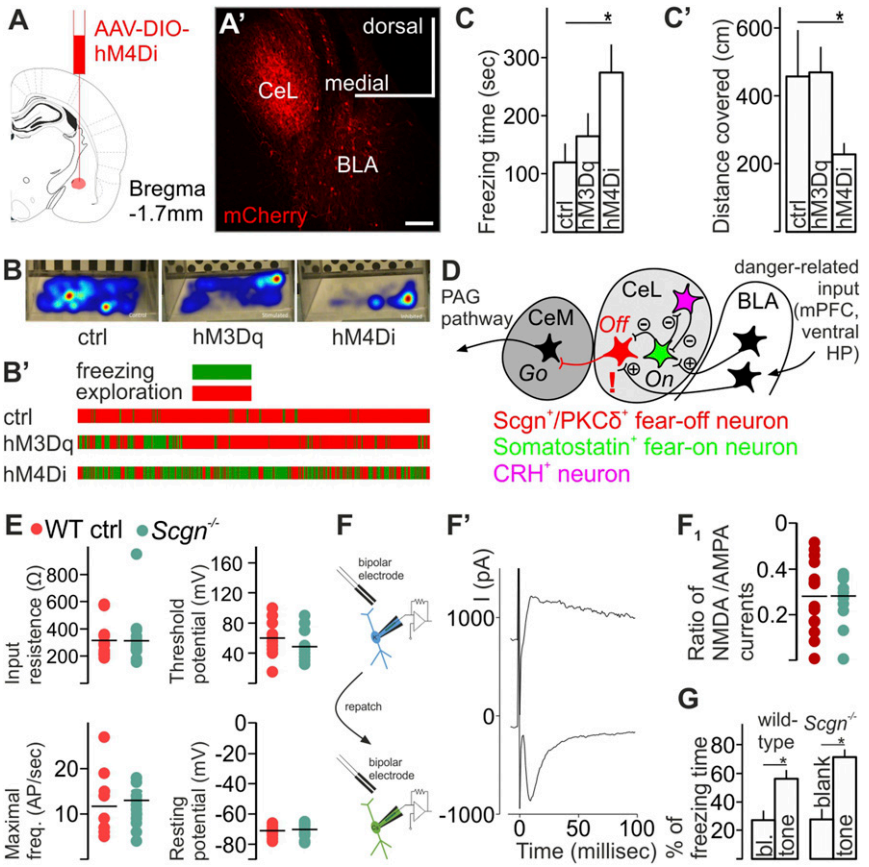

Fig. 2. Secretagogin (Scgn) labels fear-off neurons. (*A–C′*) Virus-mediated inhibition of CeL Scgn$^+$ cells in Scgn-Cre mice increased total freezing time but decreased the distance covered in the cage. Gantt chart visualized individual data in the different experimental groups. (*D*) Circuitry map focusing on the CeL. Exclamation mark indicates Scgn's role in excitatory synapses at Scgn$^+$/PKCδ$^+$ neurons. (*E*) Genetic ablation of Scgn did not change the electrophysiological properties of Scgn$^+$/PKCδ$^+$ CeL neurons. (*F*, *F′*, and F_1). NMDAR to AMPAR currents evoked by extracellular stimulation in WT and *Scgn*$^{-/-}$ mice after aversive danger conditioning. To calculate the ratio, AMPA currents were measured at peak amplitude of current evoked at −80 mV holding potential; NMDA currents were estimated at 40 ms after stimulation (V_h = +60 mV). No genotype effect was identified. (*G*) *Scgn*$^{-/-}$ mice showed no difference in the percentage of total freezing time after aversive danger conditioning (n = 5 KO and n = 9 WTs, P = 0.24, Student's t test). Both WT and *Scgn*$^{-/-}$ mice showed increased percentage of time spent freezing during the presentation of the conditioned stimulus (tone) as compared to the equvivalent time period before the onset of the tone; no differences between genotypes were detected. BLA, basolateral amygdala; CeL, centrolateral nucleus of amygdala; CeM, centromedial amygdala, ctrl control.

proteomic data from olfactory and rostral migratory areas and found the GluN2B invariably present in the Scgn interactome (33). Next, we substantiated a likely Scgn–GluN2B interaction by immunoprecipitating protein complexes with an anti-Scgn antibody (Fig. 3*B*) in total amygdala homogenates. A Scgn–GluN2B interaction was sensitive to and correlated with prior fear conditioning (*SI Appendix*, Fig. S5*B*). Nano-resolved fluorescence microscopy from primary amygdala cultures indicated that Scgn is sequestered at submembranous sites where GluN2 accumulates/transits to the postsynaptic density, at least in vitro (Fig. 3 *C–F″*). At the ultrastructural level, Scgn concentrated in postsynaptic dendrite stretches of asymmetrical synapses (Fig. 3 *G* and *G′*). Together these data suggest that Scgn could modulate excitatory neurotransmission by tuning the availability of the GluN2B NMDAR subunit.

Scgn Modulates GluN2B Availability on the Membrane Surface In Vitro. We hypothesized that Scgn could participate in allowing delivery of GluN2B subunits to the plasma membrane. To test this hypothesis, we took advantage of SuperEcliptic pHluorine (SEP) (34) labeling, which emits fluorescence only when the mutant GFP tag is exposed to the extracellular pH in living cells (35). Human-derived SH-SY5Y cells natively expressing Scgn were transfected with a plasmid encoding the GluN2B subunit tagged with SEP on its N-terminal extracellular extremity in combination (or not) with *Scgn* knockdown (*Scgn*^{KD}). Baseline fluorescence intensity of the SEP-GluN2B signal was significantly lower in *Scgn*^{KD} cells (Fig. 4*A*; n = 15 control and n = 8 Scgn^{KD} cells; $P < 0.05$, Shapiro–Wilk test and Student's t test). Furthermore, postbleaching FRAP recovery revealed that signal recovery in bleached membrane segments was significantly slower after *Scgn*^{KD} (Fig. 4*B*, recovery half time values of the averaged FRAP curves were 89.9 and 102.7 s for control and *Scgn*^{KD} cells [n = 10 control and n = 9 Scgn^{KD} cells; $P < 0.05$, Mann–Whitney test or Student's t test], respectively). Additionally, *Scgn*^{KD} reduced the recovery plateau (from 69.82 s in control to 55.29 s in *Scgn*^{KD}; n = 10 control and n = 9 Scgn^{KD} cells; $P < 0.05$, Mann–Whitney test or Student's t test), respectively), which indicates impaired recovery of membrane fluorescence. Reduced SEP-GluN2B surface signal was not due to a lower amount of cellular GluN2B subunits in *Scgn*^{KD} neurons: while acid treatment equally abolished all surface fluorescence, application of NH_4Cl reinstated identical whole-cell SEP-GluN2B signal intensity in both control and *Scgn*^{KD} SH-SY5Y cells (Fig. 4 *C–E*; n = 3 well each, $P < 0.05$, Shapiro–Wilk test and Student's t test).

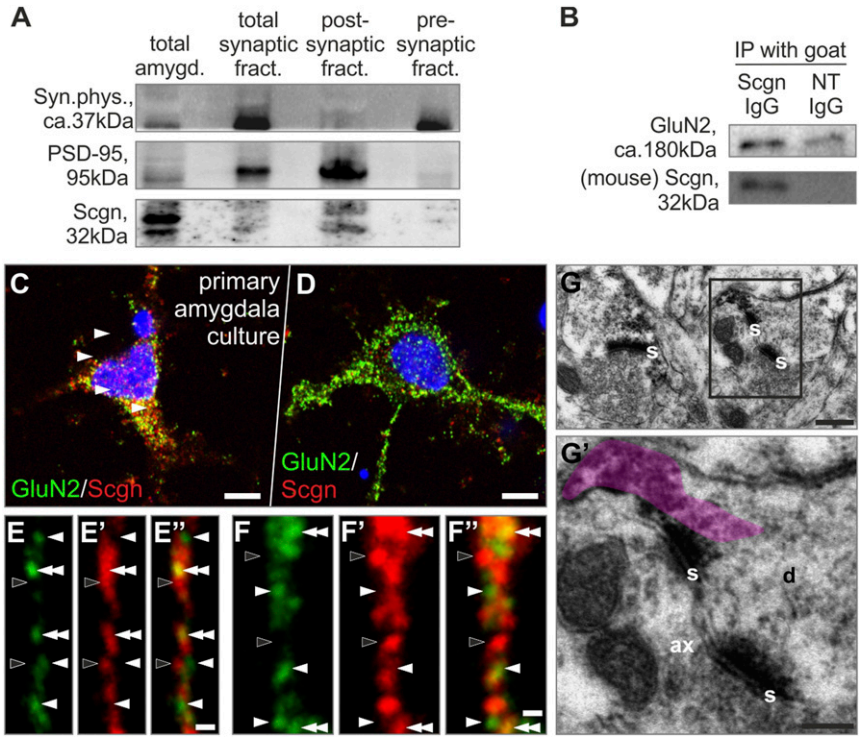

Fig. 3. Secretagogin (Scgn) concentrates in the postsynaptic compartment of excitatory synapses. (*A*) Western blotting showed Scgn expression in the postsynaptic density fraction of amygdala punches. (*B*) GluN could be immunoprecipitated with an anti-Scgn antibody from amygdala punches. (*C* and *D*) GluN2$^+$ neurons of primary amygdala culture could coexpress Scgn. (*E–F″*) High-resolution airyscan imaging of GluN2$^+$/Scgn$^+$ neurons revealed close apposition of GluN2$^+$ (white arrowheads) and Scgn$^+$ (black arrowheads) puncta with colocalizations (double arrowheads). (*G* and *G′*) Scgn typically condensed in the postsynaptic compartment (immunoprecipitate semitransparently color-coded in violet). ax, axon; d, dendrite; GluN2, NMDA receptor 2 subunit; IP, immunoprecipitation; NT, IgG non-target immunoglobulin G; PSD-95, postsynaptic density protein 95; s, synapse. (Scale bars: *C* and *D*, 5 μm; *E″* and *F″*, 1 μm; *G*, 100 nm; *G′*, 70 nm.)

GluN2B is phosphorylated at its 1,472 tyrosine residue (Tyr-1472) upon binding in the postsynaptic density to enhance the ability of functional NMDARs to regulate Ca^{2+} influx in response to glutamate (36). *Scgn*^{KD} decreased GluN2B phosphorylation at Tyr-1472 (Fig. 4 *F* and *F′*; $n = 3$ wells each, $P < 0.05$, Student's t test). The total amount of GluN2B mRNA/protein did not change however ($P > 0.05$, Student's t test). This finding implicates Scgn in modulating GluN2B surface availability in the cell membrane (36) without affecting the total amount of GluN2B.

Discussion

The amygdala is a central node of a subcortical defensive survival circuit, which shapes behavioral responses to threatening stimuli (37, 38). In contrast to its cortex-like lateral structures, which contain mainly glutamatergic neurons (39), its medial structures—forming the central nuclei—are principally composed of GABAergic interneurons (40). Inhibition is critical to shape and synchronize network activity (41). Accumulating evidence indicates that local inhibitory circuits mediate important aspects of fear conditioning in the amygdala: Local treatments that increase GABA neurotransmission reduce conditioned threat responses (42). Likewise, inhibitory neurons are major targets of neuromodulators/neuropeptides (43, 44), which typically fine-tune neuronal activity. The functional segregation of the central amygdala as a command module gained momentum when fear-on (CeL_{on}) and fear-off (CeL_{off}) cell pools were identified to trigger or block, respectively, fear conditioning driven by the engagement of a local inhibitory microcircuit that gates CeM output to control the level of conditioned freezing (10, 15, 45). However, neuron-specific molecular machineries, which shape experience-dependent learning remained largely unexplored.

While Scgn$^+$ neurons occur in practically all amygdala nuclei, including the extended amygdala (21), we focused on the dense Scgn$^+$ cell group in the CeL, which coexpresses PKCδ. PKCδ$^+$ interneurons were identified as CeL_{off} cells, which inhibit CeM output neurons, hence, reduce freezing (10). We hypothesized that Scgn is involved in the learning process of the behavioral responses to perceived danger but not in stress situations that lack a conditioning stimulus. Indeed, Scgn$^+$ cells form a mutually exclusive population with CRH$^+$ cells, the latter being typically activated by unconditioned stress (10). Of note, in the present animal study we were investigating nonconscious behavioral responses to threat and have largely sought to avoid the term "fear" and its association to conscious mental processes in people (2). However, when referring to other studies, we have opted to employ the terminology used in the original descriptions.

Using cell-specific chemogenetic inhibition of Scgn$^+$ CeL neurons, we showed an enhancement of conditioned freezing. We argue that the effect is due to the inhibition of a subset of PKCδ$^+$/Scgn$^+$ CeL_{off} interneurons and, thus, disinhibition of output CeM neurons (10). Recently, PKCδ$^+$ CeL neurons were reported to control learning through regulating synaptic strengthening onto lateral amygdala neurons (11). This latter study revised the prevailing model that all PKCδ$^+$ cells are fear-off neurons. Instead, they argued that PKCδ$^+$ cells represent a heterogeneous population since they identified CeL PKCδ$^+$ cells as actually being fear-on. Here, we identify Scgn$^+$/PKCδ$^+$ CeL neurons as a subpopulation of PKCδ$^+$ cells, which gate learned

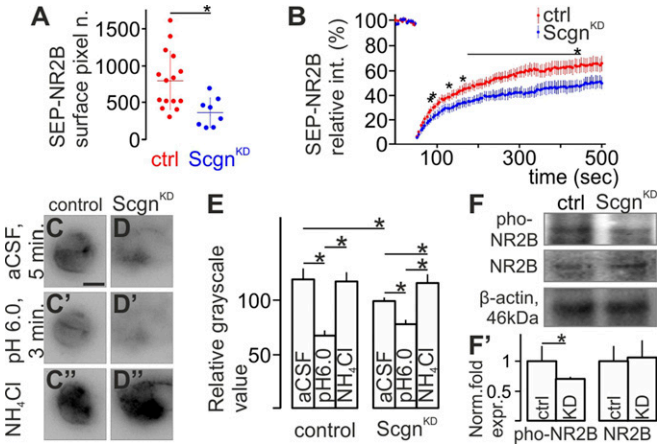

Fig. 4. Secretagogin (Scgn) shapes surface availability in the cell membrane. (*A*) Scgn silencing decreased the initial fluorescence intensity of the SEP-GluN2B signal in transfected SHSY5Y cells. (*B*) FRAP curves show slower signal recovery in Scgn-silenced ($Scgn^{KD}$) cells. (*C* and *C″*) SEP-GluN2B signal decreased at pH 6.0 but recovered both in the surface plasma membrane and within the cell in SHSY5Y cells. (*D–D‴* and *E*) $Scgn^{KD}$ reduced SEP-GluN2B signal under control medium conditions (artificial cerebrospinal fluid, aCSF). Acid treatment decreased, whereas application of NH_4Cl recovered SEP-GluN2B signal intensity in both control and $Scgn^{KD}$ cells. Note the increase between after NH_4Cl treatment compared to control medium condition after $Scgn^{KD}$ only. (*F* and *F′*) Scgn silencing decreased GluN2B phosphorylation at the Tyr-1472 residue (pho-NR2B) in SHSY5Y neuroblastoma cells leaving the total amount of GluN2B unchanged. CeL, centrolateral nucleus of amygdala; ctrl, control.

behavioral threat responses and originally were classified as CeL_{off} cells, and provide information on the subcellular localization of Scgn and on the molecular mechanisms of action involved.

The subnuclei of the amygdala play complementary roles in the acquisition and expression of threat-induced behavior. Learned association requires plasticity; this critical process has been typically related to the LA, while information modulation and subsequent output was attributed to the CeA, especially to its medial division, CeM (46). Recent advances suggest however that plasticity does occur within the CeA and that these small-scale functional changes contribute to dynamic shaping of danger-induced behavior, an assumption which has been challenged at the level of genetically defined interneurons. Particular interest turned on CeL because of the primary composition of its local inhibitory neurons: $SOM^+/PKC\delta^-$ neurons were identified as the cellular loci of synaptic plasticity in this select amygdala domain. SOM^+ neurons showed increases in the frequencies and amplitudes of their miniature excitatory postsynaptic potentials, signs of plastic changes, after fear conditioning (47). Similarly, long-term potentiation could be evoked in the LA-to-CeL pathway and shifts in the excitability of CeL neurons were attributed to activity-dependent strengthening of SOM^+ cell output as postsynaptic target (45). In turn, $SOM^-/PKC\delta^+$ CeL neurons were shown to be responsible for tonic inhibition of the CeM and to convey disinhibition from SOM^+ CeL cells in threat-avoidance behavior (7). Here, we show that lack of Scgn does not change the electrophysiological properties of $Scgn^+/PKC\delta^+$ CeL cells, nor does it affect the ratio of functionally active NMDA channels postsynaptically after aversive danger conditioning, likely pointing to tonic and redundant processes operating at slower timescales than Scgn manipulation in vitro.

CeL neurons receive excitatory input from glutamatergic neurons of the BLA, which signal through NMDARs (1), placing Scgn into the postsynaptic domain and suggesting that Scgn could regulate cell activation through affecting NMDAR availability. Functional NMDARs are tetramers composed of two essential GluN1 subunits in tandem with two GluN2 subunits (or alternatively a GluN2 and a GluN3 subunit) (48). GluN2B subunits are critical: Through interacting with postsynaptic density protein 95 (PSD95) (49), they are key regulators of NMDAR trafficking (50), ensuring sufficiently fast recycling and warranting surface mobility (51). Based on our previous mass spectrometry data (33), we specify GluN2B subunits as interactive partners of Scgn and suggest that Scgn facilitates the delivery of NMDARs to the plasma membrane: FRAP microscopy showed that the loss of Scgn impairs membrane-directed trafficking of the GluN2B subunit and Western blot analysis proved decreased Tyr-1472 phosphorylation, reflecting reduced binding to, and overt stability in, the subsynapse (36). We biochemically identified an increase in Scgn–GluN2B interaction locally in the amygdala after aversive danger conditioning, too. We interpret this seemingly contradictory finding as a compensatory mechanism, which can balance a highly excited amygdala during the investigated conditioning task in Scgn CeL_{off} neurons.

Conclusively, we explored a domain- and cell-specific molecular mechanism in the CeL. We classified a select neuron population in the CeL, which gates danger response and explored the role of a Ca^{2+}-sensor protein in the postsynaptic machinery to regulate NMDAR/GluN2B availability.

Materials and Methods

Animals, Surgery, and Ethical Approval of Experimental Studies. A total of 34 male rats (Wistar, 12 wk old), 20 fetuses on embryonic day 20 from 3 dams and 20 mice of both sexes (5–6 mo old) were used. *Scgn*-GFP mice were developed using bacterial artificial chromosome engineering technology (52). $Scgn^{-/-}$ mice were custom-generated at Mutant Mouse Resource & Research Centers (Mouse Biology Program, University of California) using the "two-in-one" targeting strategy (53), which generates full knockouts by expressing a termination signal after exon 3 of the secretagogin gene. CRH-GFP reporter mice (all females, $n = 3$, 19 wk of age) were generated using bacterial artificial chromosome technology (26). Food and water were available ad libitum. Animals were kept under standard housing conditions with a 12/12 light/dark cycle (lights on at 0800; 55% air humidity). Experimental procedures, including stereotaxic injections and transcardial perfusion, were approved by the Ethical Review Boards of the Semmelweis University (Protocols: ETS 170 and 123) and the Medical University of Vienna/the Austrian Ministry of Science and Research (66.009/0145-WF/II/3b/2014 and 66.009/0277-WF/V/3b/2017) and conformed to the 2010/63/European Union European Communities Council Directive. During experimental manipulation of live animals, these were anesthetized intramuscular or intraperitoneal with a mixture of ketamine (50 mg/kg body weight) and xylazine (4 mg/kg body weight). After surgery, brains were perfusion-fixed by transcardially applying 4% (wt/vol) paraformaldehyde in 0.1 M phosphate buffer. In vivo track tracing, formalin stress, fear conditioning, and the microinjections of viral particles for cell type-specific targeting in *Scgn*-Cre mice are in *SI Appendix, Materials and Methods*.

Human Subjects. For immunohistochemistry, two in situ perfused brains were used (*SI Appendix*, Table S1). Tissues were obtained and used in compliance with the Declaration of Helsinki and followed relevant institutional guidelines (Regional and Institutional Committee of Science and Research Ethics of Semmelweis University [TUKEB 84/2014]). Patient material was coded to maintain anonymity throughout tissue processing. Procedural details are described in *SI Appendix, Materials and Methods*.

Immunohistochemistry and Morphometry. Chromogenic or multiple immunofluorescence histochemistry with select combinations of primary antibodies (*SI Appendix*, Table S2) was performed according to published protocols (20, 21, 31, 33, 54–59). Images of specimens after processing for chromogenic histochemistry were captured on an Olympus BX-51 microscope. Sections processed for multiple immunofluorescence histochemistry were inspected and corresponding images were acquired on an LSM780 confocal laser-scanning microscope (Zeiss). Superresolution images (~60 nm axial resolution) were acquired on a LSM880 laser-scanning microscope equipped with an "Airyscan" detector system. Human sections were analyzed and diagrammed using Neurolucida. Details of the procedures are referred to in *SI Appendix, Materials and Methods*.

Electron Microscopy. Sections processed for postembedding Scgn immunohistochemistry with DAB-NI detection were postfixed, contrasted in buffered 1% OsO_4 at 22–24 °C for 1 h, and flat-embedded in Durcupan ACM (Fluka). The CeL was excised and reembedded for ultrasectioning at 100-nm thickness. Sections were collected on single-slot nickel grids coated with Formvar and studied on a Jeol 1200 EMX microscope. Primary magnification ranged from 20,000× to 80,000×, as indicated.

Electrophysiology. To prepare slices for patch-clamp experiments, we used a protective recovery method as described previously (31, 60). Briefly, deeply anesthetized mice were transcardially perfused with 20 mL of chilled oxygenated (95% O_2/5% CO_2) solution containing (in mM): 93 *N*-methyl-D-glutamine-HCl, 30 $NaHCO_3$, 2.5 KCl, 1.2 NaH_2PO_4, 20 Hepes-NaOH, 5 Na-ascorbate, 3 Na-pyruvate, 0.5 $CaCl_2$, 8 $MgSO_4$, and 25 glucose (pH 7.4). Brains were rapidly extracted, immersed in the same solution, and cut into 300-μm thick coronal slices with Leica VT1200S vibratome. The slices containing the amygdala were then transferred to a recovery chamber filled with the same solution (32 °C) for 12 min and later kept (minimum 60 min prior to the recordings) in a solution containing (in mM): 90 NaCl, 26 $NaHCO_3$, 3 KCl, 1.2 NaH_2PO_4, 20 Hepes-NaOH, 5 Na-ascorbate, 3 Na-pyruvate, 1.5 $CaCl_2$, 2 $MgSO_4$, 0.5 L-glutatione, and 25 glucose (pH 7.4) (31).

To define electrophysiological profiles, current clamp recordings on cells from the central amygdala (lateral part) were performed in oxygenated (95% O_2/5% CO_2) artificial CSF containing (in mM): 124 NaCl, 2.5 KCl, 2 $MgCl_2$, 1.5 $CaCl_2$, 24 $NaHCO_3$, 1.2 NaH_2PO_4, 5 Hepes, and 12.5 glucose. Pipettes of 3–5 MΩ resistance contained (in mM): 120 K-gluconate, 6 KCl, 10 Hepes-KOH, 5 EGTA, 4 ATP-Mg, 0.3 GTP (pH was adjusted to 7.3 with KOH). Perfusion speed was set to 2.5/min (31).

To measure NMDA/AMPA ratio (30), we repatched the cells of interest (i.e., demonstrating late-firing electrophysiological profile) with the pipette containing (in mM): 140 CsCl, 4 NaCl, 2 $MgCl_2$, 10 Hepes, 1 EGTA, 4 ATP-Na2, 0.3 GTP (pH was adjusted to 7.3 with NaOH). Additionally, picrotoxin (20 μm) was added to the extracellular solution to block GABAA receptors. For neuronal stimulation, a bipolar electrode was placed at the ventrolateral part of the central amygdala where the BLA-CeA pathway enters (61) and was programmable activated to shortly (0.1–0.7 ms) generate 100–250 μA current.

Cell Lines and Primary Neuronal Culture. SH-SY5Y cells were kept in DMEM:-GlutaMax containing 5% fetal bovine serum, penicillin (100 U/mL), and streptomycin (100 μg/mL; all from Invitrogen). Cells were trypsin dissociated and plated at a density of 50,000 cells per well in 24-well plates for morphometry and at a density of 2×10^6 cells per well in six-well plates for Western blot analysis. Primary neuronal cultures were made from newborn (P0) rat brains' amygdala and processed for immunohistochemistry. *Scgn* gene silencing was through the application of a mixture of Scgn-specific small interfering RNAs (siRNAs) (250 pmol/500 μL, diluted in culture medium; GE Dharmacon) for 2 d (33).

Western Blotting. Protein samples from the amygdala of rats in control or after fear conditioning ($n = 6$ per group) were prepared, and their concentrations were determined (62). Protein samples were analyzed under denaturing conditions (*SI Appendix*, Fig. S6). Western blotting was performed with the primary antibodies listed in *SI Appendix*, Table S2. Blots were scanned on a Bio-Rad XRS$^+$ imaging system and subsequently quantified in Image Lab 3.01 (Bio-Rad Laboratories). β-Actin (1:10.000; Sigma) was used as loading control.

Immunoprecipitation. We followed previously published protocols (31). Amygdala samples of fear-conditioned and sham-trained rats were isolated immediately after training and collected in lysis buffer containing 50 mM NaCl, 20 mM Hepes, 10 μM $CaCl_2$, 0.2% Triton X-100, and a mixture of protease inhibitors (Roche; pH was adjusted to 7.4). Tissues were homogenized by ultrasonication, centrifuged at 18,000 × *g* for 30 min, with the supernatants used for experimentation. After preclearance using Protein G-coated Dynabeads (Novex; Life Technologies, 45 min), samples (50 μL) were incubated with goat anti-Scgn primary antibody (1:2,000, R&D Systems) overnight at 4 °C. An aliquot of each sample was then probed simultaneously with goat IgG (2 μg/50 μL) to control for nonspecific binding. Subsequently, samples were incubated with Dynabeads for 90 min. After repeated rinses, Dynabeads were collected, bound proteins eluted with Laemmli buffer, and separated on 10% resolving gels under denaturing conditions (sodium dodecyl sulfate–polyacrylamide gel electrophoresis).

Preparation of Synaptosomal Fractions and Enrichment in Postsynaptic Densities. Rat amygdala punches were homogenized in 0.32 M sucrose-containing Hepes buffer (in mM: 145 NaCl, 5 KCl, 2 $CaCl_2$, 1 $MgCl_2$, 5 glucose, and 5 Hepes at pH 7.4), centrifuged (600 × *g*, 10 min at 4–8 °C) and the supernatant repeatedly cleared (by centrifugation at 20,000 × *g*, 4 °C for 30 min in 1.3 M sucrose-containing Hepes buffer) (63). To enrich postsynaptic densities (PSDs), rat amygdala samples were homogenized in 0.32 M sucrose solution (containing 1 mM $NaHCO_3$, 1 mM $MgCl_2$, 0.5 mM $CaCl_2$, 1 mM phenylmethylsulfonyl fluoride, and protease inhibitors [Roche, cOmplete]), the homogenates centrifuged (470 × *g*, 2 min at 4 °C) and supernatants centrifuged (10,000 × *g*, 10 min at 4 °C). Soluble protein-containing supernatants were resuspended in 0.32 M sucrose, which were then layered onto 0.8 M sucrose. After being centrifuged at 9,100 × *g* (4 °C for 15 min) synaptosome-containing pellets were collected from 0.8 M sucrose layer and resuspended with equal volume of 20 mM Hepes (pH 7.0), 2% Triton X-100, and 150 mM KCl. Samples were centrifuged at 20,800 × *g* (45 min at 4 °C), and resulting pellets were resuspended in a solution of 1% Triton X-100 and 75 mM KCl, and centrifuged again (20,800 × *g*, 30 min at 4 °C) to yield the "PSD fraction" (64).

FRAP Combined with Gene Silencing. Live-cell imaging was carried out on SHSY-5Y cells transfected with 0.5 μg of pCI-SEP_NR2B plasmid DNA (Addgene 23998), and Scgn subsequently silenced with siRNA as above. Fluorescence recovery of NR2B-SEPs destined to the cell surface after photobleaching was recorded by a Zeiss CellObserver system. Procedural details of transfection and imaging are described in *SI Appendix, Materials and Methods*.

Statistics. Data were analyzed using the Statistica Software Package version 13.2 (StatSoft). Pairwise comparisons for in vitro histochemical and Western blotting experiments were performed by Student's *t* test (on independent samples). Data were normalized to control if and when necessary. Data were expressed as means ± SEM. A *P* value of <0.05 was considered statistically significant. For FRAP experiments, average fluorescence intensity during postbleach fluorescence recovery was compared in each time point using IBM SPSS Statistics software. After determining the distribution of the data in the time points by Shapiro–Wilk's test of normality, Student's *t* test was used to compare normally distributed and Mann–Whitney test to compare nonnormally distributed data. Initial membrane intensities were normally distributed and thus compared by Student's *t* test.

Data Availability. All study data are included in the article and/or *SI Appendix*.

ACKNOWLEDGMENTS. We thank N. Hájos for sharing an anti-PKCδ antibody and extensive discussions; P. Rebernik for excellent technical assistance; L. Wagner for anti-secretagogin antibodies; F. Erdelyi, G. Szabo, and Z. Mate for the custom generation of *Scgn*-GFP and *Scgn*-Cre mice; J. Petersen for help with FRAP microscopy; and M. Courtney for advice on GluN2B constructs. Lisa E. Pomeranz and Kaamashri N. Latcha (The Rockefeller University) are acknowledged for providing brain tissues from *Crh*-GFP mice. This work was supported by National Brain Research Program of Hungary Grants 2017-1.2.1-NKP-2017-00002 (to A.A.), KTIA_NAP_13-1-2013-0001 (to M.P.), and 2017_1.2.1-NKP-2017-00002 (to K.S.); Excellence Program for Higher Education of Hungary Grant FIKP-2018 (to A.A.); Advanced EMBO Fellowship Grant EMBO ALTF 493-2017 (to R.A.R.); National Research, Development and Innovation Office of Hungary Grant VEKOP-2.3.3-15-2016-00007 and Eötvös Loránd University Thematic Excellence Programme 2020 supported by National Research, Development and Innovation Office Grant TKP2020-IKA-05 (to K.S.); Austrian Science Fund (Grants P28683 and P30461 to D.D.P.); the Swedish Research Council (T.H. and T.G.M.H.); Hjärnfonden (T.H.); and the European Research Council SECRET-CELLS (Grant ERC-2015-AdG-695136 to T.H.).

1. I. Ehrlich *et al*., Amygdala inhibitory circuits and the control of fear memory. *Neuron* **62**, 757–771 (2009).
2. J. E. LeDoux, Coming to terms with fear. *Proc. Natl. Acad. Sci. U.S.A.* **111**, 2871–2878 (2014).
3. J. E. Krettek, J. L. Price, A description of the amygdaloid complex in the rat and cat with observations on intra-amygdaloid axonal connections. *J. Comp. Neurol.* **178**, 255–280 (1978).
4. C. Herry, J. P. Johansen, Encoding of fear learning and memory in distributed neuronal circuits. *Nat. Neurosci.* **17**, 1644–1654 (2014).
5. P. Veinante, M. J. Freund-Mercier, Intrinsic and extrinsic connections of the rat central extended amygdala: An in vivo electrophysiological study of the central amygdaloid nucleus. *Brain Res.* **794**, 188–198 (1998).
6. R. M. Sears, H. C. Schiff, J. E. LeDoux, Molecular mechanisms of threat learning in the lateral nucleus of the amygdala. *Prog. Mol. Biol. Transl. Sci.* **122**, 263–304 (2014).

7. O. P. Keifer Jr, R. C. Hurt, K. J. Ressler, P. J. Marvar, The physiology of fear: Reconceptualizing the role of the central amygdala in fear learning. *Physiology (Bethesda)* **30**, 389–401 (2015).
8. R. M. Tillman *et al*., Intrinsic functional connectivity of the central extended amygdala. *Hum. Brain Mapp.* **39**, 1291–1312 (2018).
9. G. M. Gafford, K. J. Ressler, Mouse models of fear-related disorders: Cell-type-specific manipulations in amygdala. *Neuroscience* **321**, 108–120 (2016).
10. W. Haubensak *et al*., Genetic dissection of an amygdala microcircuit that gates conditioned fear. *Nature* **468**, 270–276 (2010).
11. K. Yu *et al*., The central amygdala controls learning in the lateral amygdala. *Nat. Neurosci.* **20**, 1680–1685 (2017).
12. A. E. Wilensky, G. E. Schafe, M. P. Kristensen, J. E. LeDoux, Rethinking the fear circuit: The central nucleus of the amygdala is required for the acquisition, consolidation, and expression of pavlovian fear conditioning. *J. Neurosci.* **26**, 12387–12396 (2006).
13. R. D. Samson, S. Duvarci, D. Paré, Synaptic plasticity in the central nucleus of the amygdala. *Rev. Neurosci.* **16**, 287–302 (2005).
14. G. D. Petrovich, L. W. Swanson, Projections from the lateral part of the central amygdalar nucleus to the postulated fear conditioning circuit. *Brain Res.* **763**, 247–254 (1997).
15. S. Ciocchi *et al*., Encoding of conditioned fear in central amygdala inhibitory circuits. *Nature* **468**, 277–282 (2010).
16. R. O. Tasan *et al*., The role of neuropeptide Y in fear conditioning and extinction. *Neuropeptides* **55**, 111–126 (2016).
17. J. P. Fadok *et al*., A competitive inhibitory circuit for selection of active and passive fear responses. *Nature* **542**, 96–100 (2017).
18. P. H. Janak, K. M. Tye, From circuits to behaviour in the amygdala. *Nature* **517**, 284–292 (2015).
19. A. Alpár, J. Attems, J. Mulder, T. Hökfelt, T. Harkany, The renaissance of Ca2+-binding proteins in the nervous system: Secretagogin takes center stage. *Cell. Signal.* **24**, 378–387 (2012).
20. R. A. Romanov *et al*., A secretagogin locus of the mammalian hypothalamus controls stress hormone release. *EMBO J.* **34**, 36–54 (2015).
21. J. Mulder *et al*., Secretagogin is a Ca2+-binding protein identifying prospective extended amygdala neurons in the developing mammalian telencephalon. *Eur. J. Neurosci.* **31**, 2166–2177 (2010).
22. B. M. De Oca, J. P. DeCola, S. Maren, M. S. Fanselow, Distinct regions of the periaqueductal gray are involved in the acquisition and expression of defensive responses. *J. Neurosci.* **18**, 3426–3432 (1998).
23. A. J. McDonald, Neurons of the lateral and basolateral amygdaloid nuclei: A golgi study in the rat. *J. Comp. Neurol.* **212**, 293–312 (1982).
24. N. H. Kalin, L. K. Takahashi, F. L. Chen, Restraint stress increases corticotropin-releasing hormone mRNA content in the amygdala and paraventricular nucleus. *Brain Res.* **656**, 182–186 (1994).
25. R. Zhang *et al*., Loss of hypothalamic corticotropin-releasing hormone markedly reduces anxiety behaviors in mice. *Mol. Psychiatry* **22**, 733–744 (2016).
26. T. Alon *et al*., Transgenic mice expressing green fluorescent protein under the control of the corticotropin-releasing hormone promoter. *Endocrinology* **150**, 5626–5632 (2009).
27. P. N. De Francesco *et al*., Neuroanatomical and functional characterization of CRF neurons of the amygdala using a novel transgenic mouse model. *Neuroscience* **289**, 153–165 (2015).
28. G. M. Alexander *et al*., Remote control of neuronal activity in transgenic mice expressing evolved G protein-coupled receptors. *Neuron* **63**, 27–39 (2009).
29. B. N. Armbruster, X. Li, M. H. Pausch, S. Herlitze, B. L. Roth, Evolving the lock to fit the key to create a family of G protein-coupled receptors potently activated by an inert ligand. *Proc. Natl. Acad. Sci. U.S.A.* **104**, 5163–5168 (2007).
30. I. Shemer *et al*., Non-fibrillar beta-amyloid abates spike-timing-dependent synaptic potentiation at excitatory synapses in layer 2/3 of the neocortex by targeting postsynaptic AMPA receptors. *Eur. J. Neurosci.* **23**, 2035–2047 (2006).
31. A. Alpár *et al*., Hypothalamic CNTF volume transmission shapes cortical noradrenergic excitability upon acute stress. *EMBO J.* **37**, e100087 (2018).
32. W. Gartner *et al*., New functional aspects of the neuroendocrine marker secretagogin based on the characterization of its rat homolog. *Am. J. Physiol. Endocrinol. Metab.* **293**, E347–E354 (2007).
33. J. Hanics *et al*., Secretagogin-dependent matrix metalloprotease-2 release from neurons regulates neuroblast migration. *Proc. Natl. Acad. Sci. U.S.A.* **114**, E2006–E2015 (2017).
34. L. Joseph, J. Augustine, M. Omana, Multilocular cystadenoma of the liver with mural nodules. *Indian J. Pathol. Microbiol.* **36**, 308–310 (1993).
35. S. Sankaranarayanan, D. De Angelis, J. E. Rothman, T. A. Ryan, The use of pHluorins for optical measurements of presynaptic activity. *Biophys. J.* **79**, 2199–2208 (2000).
36. G. Lavezzari, J. McCallum, R. Lee, K. W. Roche, Differential binding of the AP-2 adaptor complex and PSD-95 to the C-terminus of the NMDA receptor subunit NR2B regulates surface expression. *Neuropharmacology* **45**, 729–737 (2003).
37. J. E. LeDoux, Emotion circuits in the brain. *Annu. Rev. Neurosci.* **23**, 155–184 (2000).
38. J. E. LeDoux, Semantics, surplus meaning, and the science of fear. *Trends Cogn. Sci.* **21**, 303–306 (2017).
39. H. C. Pape, D. Pare, Plastic synaptic networks of the amygdala for the acquisition, expression, and extinction of conditioned fear. *Physiol. Rev.* **90**, 419–463 (2010).
40. A. J. McDonald, Cytoarchitecture of the central amygdaloid nucleus of the rat. *J. Comp. Neurol.* **208**, 401–418 (1982).
41. T. F. Freund, G. Buzsáki, Interneurons of the hippocampus. *Hippocampus* **6**, 347–470 (1996).
42. J. A. Harris, R. F. Westbrook, Effects of benzodiazepine microinjection into the amygdala or periaqueductal gray on the expression of conditioned fear and hypoalgesia in rats. *Behav. Neurosci.* **109**, 295–304 (1995).
43. C. R. Pinard, J. F. Muller, F. Mascagni, A. J. McDonald, Dopaminergic innervation of interneurons in the rat basolateral amygdala. *Neuroscience* **157**, 850–863 (2008).
44. E. Asan, The catecholaminergic innervation of the rat amygdala. *Adv. Anat. Embryol. Cell Biol.* **142**, 1–118 (1998).
45. H. Li *et al*., Experience-dependent modification of a central amygdala fear circuit. *Nat. Neurosci.* **16**, 332–339 (2013).
46. M. S. Fanselow, J. E. LeDoux, Why we think plasticity underlying Pavlovian fear conditioning occurs in the basolateral amygdala. *Neuron* **23**, 229–232 (1999).
47. M. A. Penzo, V. Robert, B. Li, Fear conditioning potentiates synaptic transmission onto long-range projection neurons in the lateral subdivision of central amygdala. *J. Neurosci.* **34**, 2432–2437 (2014).
48. S. G. Cull-Candy, D. N. Leszkiewicz, Role of distinct NMDA receptor subtypes at central synapses. *Sci. STKE* **2004**, re16 (2004).
49. R. A. Al-Hallaq, T. P. Conrads, T. D. Veenstra, R. J. Wenthold, NMDA di-heteromeric receptor populations and associated proteins in rat hippocampus. *J. Neurosci.* **27**, 8334–8343 (2007).
50. L. Bard, L. Groc, Glutamate receptor dynamics and protein interaction: Lessons from the NMDA receptor. *Mol. Cell. Neurosci.* **48**, 298–307 (2011).
51. L. Groc *et al*., NMDA receptor surface mobility depends on NR2A-2B subunits. *Proc. Natl. Acad. Sci. U.S.A.* **103**, 18769–18774 (2006).
52. D. Calvigioni *et al*., Functional differentiation of cholecystokinin-containing interneurons destined for the cerebral cortex. *Cereb. Cortex* **27**, 2453–2468 (2017).
53. W. C. Skarnes *et al*., A conditional knockout resource for the genome-wide study of mouse gene function. *Nature* **474**, 337–342 (2011).
54. D. Lendvai *et al*., Neurochemical mapping of the human hippocampus reveals perisynaptic matrix around functional synapses in Alzheimer's disease. *Acta Neuropathol.* **125**, 215–229 (2013).
55. E. Renner, N. Puskás, A. Dobolyi, M. Palkovits, Glucagon-like peptide-1 of brainstem origin activates dorsomedial hypothalamic neurons in satiated rats. *Peptides* **35**, 14–22 (2012).
56. I. M. Gut *et al*., Novel application of stem cell-derived neurons to evaluate the time- and dose-dependent progression of excitotoxic injury. *PLoS One* **8**, e64423 (2013).
57. R. Hua, S. Yu, M. Liu, H. Li, A PCR-based method for RNA probes and applications in neuroscience. *Front. Neurosci.* **12**, 266 (2018).
58. T. Bullmann *et al*., Tau phosphorylation-associated spine regression does not impair hippocampal-dependent memory in hibernating golden hamsters. *Hippocampus* **26**, 301–318 (2016).
59. A. Alpár *et al*., Endocannabinoids modulate cortical development by configuring Slit2/Robo1 signalling. *Nat. Commun.* **5**, 4421 (2014).
60. S. Zhao *et al*., Cell type–specific channelrhodopsin-2 transgenic mice for optogenetic dissection of neural circuitry function. *Nat. Methods* **8**, 745–752 (2011).
61. Y. Fu, P. Shinnick-Gallagher, Two intra-amygdaloid pathways to the central amygdala exhibit different mechanisms of long-term potentiation. *J. Neurophysiol.* **93**, 3012–3015 (2005).
62. M. M. Bradford, A rapid and sensitive method for the quantitation of microgram quantities of protein utilizing the principle of protein-dye binding. *Anal. Biochem.* **72**, 248–254 (1976).
63. P. K. Kamat, A. Kalani, N. Tyagi, Method and validation of synaptosomal preparation for isolation of synaptic membrane proteins from rat brain. *MethodsX* **1**, 102–107 (2014).
64. A. Dosemeci, J. H. Tao-Cheng, L. Vinade, H. Jaffe, Preparation of postsynaptic density fraction from hippocampal slices and proteomic analysis. *Biochem. Biophys. Res. Commun.* **339**, 687–694 (2006).